



Contents lists available at ScienceDirect

International Journal of Rock Mechanics and Mining Sciences

journal homepage: www.elsevier.com/locate/ijrmms

Preliminary study on the feasibility of co-exploitation of coal and uranium

Guanglei Cui^{a,b}, Jiong Wei^{c,**}, Xia-Ting Feng^{a,*}, Jishan Liu^d, Derek Elsworth^e, Tianyu Chen^a, Wei Xiong^f

^a Key Laboratory of Ministry of Education on Safe Mining of Deep Metal Mines, Northeastern University, Shenyang, 110004, China

^b Shandong Key Laboratory of Depositional Mineralization & Sedimentary Mineral, Shandong University of Science and Technology, Qingdao, 266590, China

^c Department of Engineering Mechanics and CNMM, Tsinghua University, Beijing, 100084, China

^d School of Mechanical and Chemical Engineering, The University of Western Australia, 35 Stirling Highway, Perth, WA, 6009, Australia

^e Department of Energy and Mineral Engineering, G3 Center and Energy Institute, The Pennsylvania State University, University Park, PA, 16802, USA

^f Gas Research Branch, China Coal Technology Engineering Group Chongqing Research Institute, Chongqing, 400037, China

ARTICLE INFO

Keywords:

Rock damage
Permeability model
Effective strain
Ordos basin
Top-caving mining
Room and pillar mining

ABSTRACT

Both coal and uranium resources are found in the Dongsheng area which is located in the northern part of Ordos Basin, China with the coal seam below the uranium deposit. In this paper, we attempt to study the feasibility of co-exploitation of the coal seam and the uranium deposit. The permeability evolution in strata around the coal seam are selected as the key parameter indexing the separate and safe concurrent recovery of two deposits and a novel strain-dependent permeability model is proposed covering the full deformation range of rock. The proposed model is first verified with experimental data with good fitting of the results. Then an upscaled numerical model is established considering the geology conditions of Dongsheng area. This is implemented using COMSOL Multiphysics; and the interface of COMSOL with MATLAB is used to study the damage to the rock mass. We show that (a) compared with the stress-dependent permeability model, the strain-dependent permeability model proposed in this work has the advantage that each strain value is associated with a unique permeability value; (b) The feasibility of co-exploitation of the coal seam and the uranium deposit depends on the relative distance between two resources. When the caved and fractured zone encroaches on the uranium deposit the coal seam should be abandoned. Conversely, when the uranium deposit lays in the constrained zone, the recovery of the coal seam would benefit recovery of the uranium deposit; (c) The feasibility of the co-recovery of the two resources can be optimized by the choice of mining approach. The top-caving mining approach and room-and-pillar mining approach can reduce the height of the caved and fractured zones and make the co-exploitation of the uranium and coal feasible. This work provides a new approach to investigate the feasibility of co-exploitation of uranium and coal.

1. Introduction

Uranium deposits are economically important in many parts of the world as it serves as a vital raw material for nuclear fuel.¹ These deposits are commonly detected in sandstone-hosted sedimentary basins and the recovery of uranium is often found co-located and interwoven with other resources (gas, oil and coal).^{2,3} The co-exploitation of these co-existing resources is a significant issue that is explored in this work.

Uranium (U) is a toxic heavy metal and radioactive element with its toxicity 6 orders of magnitude more harmful than its radioactivity.^{4,5} When recovered, the uranium should be retained in solid form and prevented from dissolving into aqueous solution and thereby

contaminating other resources. Issues of uranium concentrations in water following Uranium mining have been widely studied.^{6,7} However, little addresses uranium leakage during the co-exploitation of other resources such as gas, oil and coal. Atkins et al.⁵ studied uranium concentration in groundwater in a coal seam gas development region in Australia. In his study, the naturally occurring radioactive materials were located in the target geological formations. While in some sedimentary basins, the uranium and co-existing resources are not in the same strata. For example, both coal and uranium are detected in the Ordos Basin, China but at different buried depths.⁸ Some basic ideas of co-exploitation of uranium and coal seams have been proposed but remain only in the conceptual stage.⁹ In this work, the feasibility of co-exploitation of uranium and coal seam is studied both theoretically and

* Corresponding author.

** Corresponding author.

E-mail addresses: jiong.wei@foxmail.com (J. Wei), fengxiating@mail.neu.edu.cn, xia.ting.feng@gmail.com (X.-T. Feng).

numerically.

Leaching is usually applied in the recovery of uranium¹⁰ where the neutral solution should be contained within the uranium deposit. Underground mining is the main method to access the coal seam causing high-intensity strata movement and changing the properties of the adjacent strata (e.g., stress, strain and permeability).^{11,12} The stratum above the longwall mining area can be divided into a number of zones characterized by different deformation mechanisms. In some studies, four zones over the goaf are identified based on geological and geotechnical evaluations of the region: the caved zone, fractured zone, constrained zone and surface zone^{13–16} While in other studies, only three zones are identified in ascending order: the caved zone, fractured zone and bending zone.^{17–19} Empirical equations to define the height of each zone are also proposed.^{11,20} The above mentioned zones broadly describe the deformation of the stratum and changing of flowability.

The variations of stress,²¹ strain,²² displacement²³ and damage zone²⁴ after coal mining have been widely discussed. In this work we focus on the co-exploitation of uranium deposits and coal seams - whether the neutral solution would leak from the uranium is a key parameter to define the safe recovery of co-existing resources. Therefore the variation of permeability in the intervening strata is a key parameter and may be described by a suitable permeability model.^{25,26} Early models simply assumed that the permeability was a power function of effective stress.^{27,28} Permeability increases with high gas pressure and low overburden pressure.²⁹ Based on this, several popular permeability models were proposed such as the Palmer-Mansoori model and Shi-Durucau model^{30,31} with Liu et al. proposing the strain dependent permeability model.^{32,33} The mining-induced permeability anisotropy should also be considered in the permeability models as the stress redistribution in the vertical and horizontal directions are significantly different following coal mining which would lead to a varied permeability value.³⁴ To date, some anisotropic permeability models have been proposed that incorporate permeability variation in a specific directions due to the anisotropic strain³⁵ or stress³⁶ evolution. It should be noted that the above-mentioned permeability models are limited to small deformation recoverable poroelasticity response.

However, damage normally occurs during mining activities and consequently results in a great decrease in the elastic modulus and a more significant increase in permeability.³⁷ Triaxial compression tests are usually applied to investigate the damage-induced permeability.³⁸ These show that coal permeability is largely enhanced after the yield point.³⁹ In the theoretical work, the permeability evolution is assumed as a function of the damage parameter (D)⁴⁰ which is related to the damage strain undergone when the coal is damaged. The Mohr Coulomb criterion and maximum tensile stress criteria are often selected to determine whether the damage is in tension or in shear.⁴¹ In recent work, Xue et al.⁴² discussed the damage evolution law of coal under compressive stress condition and proposed a stress-dependent permeability model describing the influence of damage evolution on permeability variation. However, in this approach, two permeability values may be associated with a single stress value when the coal sample is damaged due to deformation path effects.

Previous studies indicated that the stratum above the goaf can be divided into several zones following coal mining and the deformation includes both elastic and non-elastic stages. The mechanisms of permeability evolution are totally different in these two stages and the permeability anisotropy should also be considered. In this work, a novel permeability model is proposed to investigate the permeability evolution in both elastic and non-elastic deformation zones. In the model, the permeability is defined as a function of the effective strain within the stress threshold and as a function of damage parameter (D) beyond that stress threshold. The permeability model is first verified against experimental data collected from stress-strain-permeability experiments.⁴² Then the verified model is applied to investigate the feasibility of co-exploitation of uranium deposits above a coal seam. A case study based on the geological conditions of the Ordos Basin, China is

established and three contrasting simulation scenarios are analyzed. Based on the model, the relative impacts of various coal mining approaches on the co-exploitation of the coal seam and uranium deposit are studied.

2. Conceptual model

The governing equations for fluid flow in the strata around the coal seam can be described as Darcy flow in which the velocity is proportional to the permeability. Therefore in this work, the permeability variation following coal mining is selected as an appropriate metric to index the feasibility of the co-exploitation of coal and uranium deposits. The change in permeability is related to the compaction and dilation of the fractures caused by the variation of the normal stress with additional impacts of rock damage. In this section, basic concepts of permeability evolution and permeability anisotropy are introduced.

2.1. Permeability variation due to normal stress change

The permeability in one specific direction is defined as the function of the aperture of the fracture oriented in that direction which is pirated on by the normal stress perpendicular to that direction.⁴³ For example, when the vertical stress decreases, the aperture in the horizontal direction increases and the horizontal permeability is enhanced. As mentioned above, the equilibrium state of the formation stress is redistributed during mining. The strata above the mining area can be divided into four major zones: the caved zone, fractured zone, constrained zone and surface zone as shown in Fig. 1.^{14–16} The permeability evolution is different in the four zones and can be summarized as follows: (a) The caved zone is located directly above the goaf. The rocks in this zone rupture and collapse. The permeabilities in both directions in this area increase significantly; (b) In the fractured zone immediately above the caved zone, the rocks sag downwards and consequently suffer bending, fracturing, joint opening and bed separation. As a consequence, both directional permeabilities in this zone increase³⁴; (c) In the constrained zone immediately above the goaf, the horizontal stress in this zone changes little, while the vertical stress in this zone is reduced significantly. Therefore, the vertical permeability maintains its initial state while the horizontal permeability may increase. (d) In the surface zone above the goaf, the strata drop vertically and the fractures in the vertical direction are compressed. Therefore, the permeability in the horizontal direction may remain constant with the permeability in the vertical direction decreasing. From the above discussion, it can be concluded that the permeability of rock strata within the caved zone and the fractured zone can significantly increase and as a result water, gas or other fluids in these two zones may discharge into the mining panels, threatening the safety of personnel.

2.2. Permeability variation due to rock damage

As the in-situ practice suggests, non-elastic strain (damage strain in this work) typically appears during the coal mining process. A typical deviatoric stress-strain image (Fig. 2) is used to illustrate the partition of the elastic strain and non-elastic strain.⁴⁴ These are partitioned by the post peak (strength stress of the system). In the pre-peak stage, the stress increases (slightly-nonlinearly) with the strain. In the post-peak stage, a strain-softening phenomenon occurs, and the rock is damaged. The permeability evolution in these two stages exhibits significant differences as some new fractures are generated during the damage process. Before the peak load is reached, the strain remains in the elastic range and the deformation is recoverable. After the peak load, the deformation of the coal matrix is irreversible, and damage occurs. In this stage, new fractures generate, providing new paths for fluids with the permeabilities increasing significantly in all directions.⁴⁵

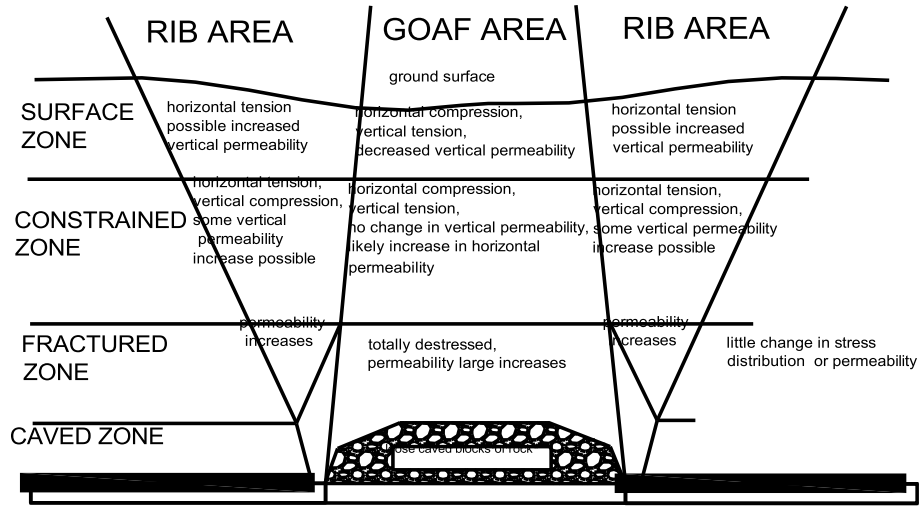


Fig. 1. Stress distribution and permeability variation after mining activities.¹⁴⁻¹⁶

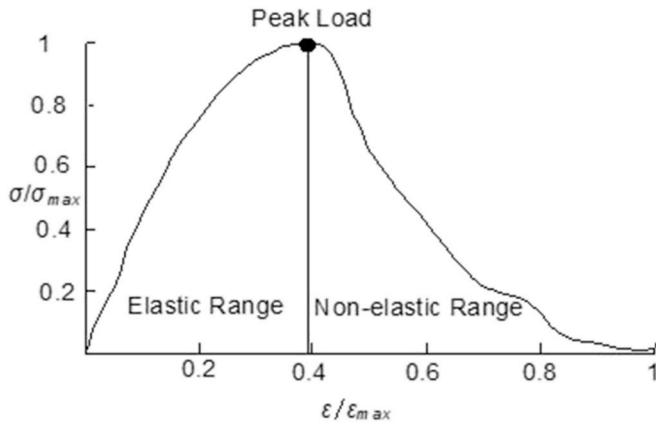


Fig. 2. The division of elastic strain and plastic strain.⁴⁴

3. Mathematical model

In this section, a mathematical model governing rock deformation, damage evolution and permeability variation is established.

3.1. Governing equation for rock deformation

Based on our previous work,^{33,46-48} the constitutive deformation relation for the porous medium is defined as:

$$Gu_{i,kk} + \frac{G}{1-2\nu}u_{k,ki} - f_f(p_m, p_f) - f_a(p_m, p_f) = f_i \quad (1)$$

where u is the displacement; G is the shear modulus; f_f is the body force caused by the fluid flow; f_a represents the body force caused by adsorption, and f_i is the other body force; p is gas pressure; Subscripts m and f represent the matrix system and fracture system, respectively.

3.2. Permeability model

3.2.1. Governing equation of the permeability

The porosity of the rock is related to the effective strain as⁴⁹:

$$\frac{\phi}{\phi_0} = 1 + \frac{\alpha}{\phi_0} \Delta \varepsilon_e \quad (2)$$

where ϕ_0 is the initial porosity, and the subscript (0) denotes the initial value of the variable; ε_e represents the effective strain in the system. In this work, the effects of gas flow and gas adsorption are neglected and

the effective strain is equal to the volumetric strain of the system:

$$\Delta \varepsilon_g = \Delta \varepsilon_v \quad (3)$$

A typical relationship between porosity and permeability is the cubic law^{46,49}:

$$\frac{k}{k_0} = \left(\frac{\phi}{\phi_0} \right)^3 = \left(1 + \frac{\alpha}{\phi_0} \Delta \varepsilon_e \right)^3 \quad (4)$$

3.2.2. Governing equation of permeability anisotropy

In this section, the equations governing the evolution of permeability anisotropy is presented. Coal can be divided into a matrix and fracture system. The flow rate in the fracture system is much higher than that in the matrix system as the fracture system supplies the main channels for gas migration. Therefore only the fracture permeability is investigated here – the matrix acting as storage. The fracture network is composed of face cleats and butt cleats.³⁵ The x - and y -directions are defined as the directions parallel to the face cleats and butt cleats, respectively. In the following section, the variation of permeability in the x -direction is taken as an example to illustrate the permeability anisotropy.

The porosity of a certain set of fractures can be obtained from the following equation³⁵:

$$\phi_{face} = \frac{b_{face}}{l_{face}} = \frac{b_{face}}{b_{face} + a_{face}} \quad (5)$$

in which a_{face} represents the matrix width and b_{face} represents the fracture aperture.

Thus we have:

$$\begin{aligned} d\phi_{face} &= d\left(\frac{b_{face}}{l_{face}}\right) = \frac{l_{face}d(l_{face} - a_{face}) - (l_{face} - a_{face})dl_{face}}{l_{face}^2} \\ &= \frac{a_{face}}{l_{face}} \left(\frac{dl_{face}}{l_{face}} - \frac{da_{face}}{a_{face}} \right) \end{aligned} \quad (6)$$

Combining Eq. (5), Eq. (6) and $1 - \phi_{face} = a_{face}/l_{face}$, the following equation is obtained:

$$\frac{d\phi_{face}}{1 - \phi_{face}} = \frac{dl_{face}}{l_{face}} - \frac{da_{face}}{a_{face}} \quad (7)$$

A Taylor expansion of the differential result is applied to Eq. (7). With the assumption that (a) the high-order terms are omitted and (b) the coal fracture porosity is much smaller than 1 ($1 - \phi_{face} \approx 1$), we can obtain³²:

$$\phi_{face} = \phi_{face0} + \frac{\Delta l_{face}}{l_{face}} - \frac{\Delta a_{face}}{a_{face}} = \phi_{face0} + \Delta \varepsilon_y^b - \Delta \varepsilon_y^m = \phi_{face0} + \Delta \varepsilon_y^{fe} \quad (8)$$

where $\Delta \varepsilon_y^b$ and $\Delta \varepsilon_y^m$ represent the linear strain variations of the coal bulk and coal matrix in the y-direction, respectively. The former term represents the global strain of the coal and the later term represents the local strain of the matrix. The superposition of these two terms is the effective strain ($\Delta \varepsilon_y^{fe}$) as defined in our previous work.³² Based on Eq. (3), we obtain:

$$\Delta \varepsilon_y^{fe} = \Delta \varepsilon_y^{fv} \quad (9)$$

where the right part represents the volumetric strain obtained from Eq. (1).

Therefore the fracture porosity ϕ_i in the direction of the i^{th} coordinate axis can be expressed as follows:

$$\phi_i = \phi_{i0} + \Delta \varepsilon_j^{fv} \quad (i \neq j) \quad (10)$$

Then the permeability anisotropy can be defined as^{50,51}:

$$\frac{k_{fx}}{k_{fx0}} = \left(1 + \frac{\alpha_{fx}}{\phi_{fx0}} \Delta \varepsilon_y^{fe} \right)^3 \quad (11.a)$$

$$\frac{k_{fy}}{k_{fy0}} = \left(1 + \frac{\alpha_{fy}}{\phi_{fy0}} \Delta \varepsilon_x^{fe} \right)^3 \quad (11.b)$$

3.3. Damage criterion for rock

The maximum tensile stress criterion or the Mohr-Coulomb criterion is selected to determine whether the damage is in tension or shear modes, and the expression is written as (positive for tension)^{41,52,53}:

$$F_1 \equiv \sigma_1 - f_{t0} = 0 \quad \text{or} \\ F_2 \equiv -\sigma_3 + \sigma_1 [(1 + \sin \varphi)/(1 - \sin \varphi)] - f_{c0} = 0 \quad (12)$$

where f_{t0} and f_{c0} are uniaxial tensile and compressive strengths respectively. φ is the internal frictional angle, and F_1 and F_2 are the two damage threshold functions used to link tension and shear damage.

According to the principle of elastic damage, the elastic modulus of an element degrades monotonically as damage evolves, and the elastic modulus of the damaged material is expressed as:

$$E = (1 - D)E_0 \quad (13)$$

where D represents the damage variable, which lies between 0 and 1, and E and E_0 are the elastic moduli of the damaged and the undamaged materials.

The evolution of the damage variable (D) is defined as follows. When a uniaxial tension experiment is conducted, the initial-strain is linearly elastic, and no damage occurs ($D = 0$). In this situation $\varepsilon < \varepsilon_{t0}$ where ε_{t0} is the tensile strain at the elastic limit as illustrated in Fig. 3. As the maximum tensile stress criterion is reached ($F_1 = 0$), damage evolves and a power function is used to describe the softening process until the residual stress (f_{tr}) is obtained. The residual stress is given as $f_{tr} = \lambda_c f_{t0} = \lambda_c E_0 \varepsilon_{t0}$ and λ_c is the residual strength coefficient, defined as the rate of the residual tensile strength f_{tr} to the initial tensile strength of the rock f_{t0} . The rock evolves to be completely damaged and $D = 1$ when the maximum tensile strain ε_{tu} is obtained. The stress-strain curve during the uniaxial tension process is illustrated in Fig. 3 (the upper-right part) and the damage variable D can be defined as⁵²:

$$D = \begin{cases} 0 & \varepsilon < \varepsilon_{t0} \\ 1 - \left| \frac{\varepsilon_0}{\varepsilon} \right|^n & \varepsilon_{t0} < \varepsilon < \varepsilon_{tr} \\ 1 - \left| \frac{\lambda_c \varepsilon_{t0}}{\varepsilon} \right|^n & \varepsilon_{tr} < \varepsilon < \varepsilon_{tu} \\ 1 & \varepsilon_{tu} < \varepsilon \end{cases} \quad (14)$$

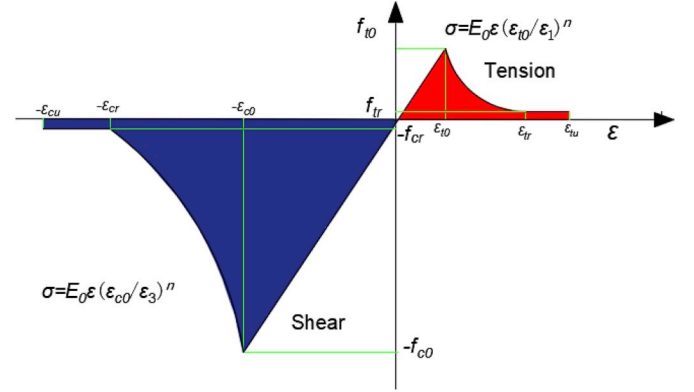


Fig. 3. The elastic damage-based constitutive law under uniaxial stress conditions.⁵⁴

The stress-strain relationship under triaxial compression is also illustrated in Fig. 3 (the lower-left part). Similar to the condition of uniaxial tension, the damage variable D can be evaluated as⁵²:

$$D = \begin{cases} 0 & \varepsilon > -\varepsilon_{c0} \\ 1 - \left| \frac{\varepsilon_0}{\varepsilon} \right|^n & -\varepsilon_{c0} > \varepsilon > -\varepsilon_{cr} \\ 1 - \left| \frac{\lambda_c \varepsilon_{c0}}{\varepsilon} \right|^n & -\varepsilon_{cr} > \varepsilon > -\varepsilon_{tu} \\ 1 & -\varepsilon_{tu} > \varepsilon \end{cases} \quad (15)$$

in which ε_{c0} is the compressive strain at the elastic limit; ε_{cu} is the maximum compressive strain, and λ_c is residual strength coefficient defined as the ratio of the residual compressive strength f_{cr} to initial compressive strength of the coal rock f_{c0} ; n is a constitutive coefficient and is set as 2 in this work.

Based on Eq. (13), the elastic modulus of the rock surrounding the coal seam declines with an increased damage variable (D). Besides the coal matrix strength, the fracture permeability also evolves as a function of the damage process.⁵² The exponential function is applied to describe the evolution of permeability with damage as⁵⁵:

$$\frac{k}{k_0} = \exp(\gamma D) \quad (16)$$

where γ is the damage-permeability coefficient indicating the effect of damage on the permeability. Note that Eq. (11) describes the permeability evolution in the pre-peak stage ($D = 0$), and the permeability anisotropy is considered. Eq. (16) describes the permeability change when damage occurs. In this situation, the permeability anisotropy is caused by the uneven distribution of stress following coal mining.

4. Model verification

Before conducting sensitivity analyses of certain field geometries, the proposed permeability model is verified against experimental data from a stress-strain-permeability experiment.⁴² The experimental procedure, results and verification results are also introduced in this section.

4.1. A triaxial compression test

Xue et al.⁴² conducted a stress-strain-permeability test with the MTS815 rock mechanics test system with a maximum axial loading capacity of 4600 kN. The coal samples were collected from No. 8 Coal Mine of the Pingdingshan Colliery in Henan Province, China. The coal samples were cylinders 50 mm in diameter and 100 mm in length. Methane was selected as the targeted gas and its pressures were set at 1, 2, and 3 MPa. The confining pressure was set at 10 MPa.

The experimental process is summarized as follows⁴²: (1) The sample was placed in the testing machine with hydrostatic pressure

applied to the coal sample at 10 MPa at a rate of 3 MPa/min; (2) The methane gas container was connected to the saturated sample with an increment of 0.25 MPa. After the gas was completely adsorbed (1, 2, 3 MPa), the initial permeability was measured using the steady state method, via the Darcy's Law; (3) The confining pressure was retained constant, while the axial pressure was increased at a rate of 10 kN/min. During this process the gas flow rate was recorded, and the permeability was calculated; (4) when the residual stage was reached, the test was completed, and the above steps were repeated with the next sample. During the loading process, stress-strain curves were recorded.

The steady state method⁵⁶ is applied to calculate the permeability value which can be written as:

$$k = \frac{2Q_0 P_0 \mu L}{A(P_1^2 - P_2^2)} \quad (17)$$

in which k is the gas permeability, Q_0 is the volumetric flow rate at the reference pressure, μ is the gas viscosity, L is the length of the coal sample, P_0 is the reference pressure, A is the cross-sectional area of the coal sample, with P_1 the upstream gas pressure and P_2 the downstream pressure.

4.2. Experiment results and verification

Because of the irreversibility of the experiment, three samples were collected for the permeability measurement and the gas pressure was maintained at 1 MPa, 2 MPa and 3 MPa, respectively. The results are shown in Fig. 4. Based on the stress-strain relationship in Fig. 3, three stages (stage I, stage II and stage III) can be observed in the experimental curve labelled as shown in Fig. 4. Stage I is the pre-peak stage, also the elastic strain stage. Stage II is in the post-peak stage before the residual strain is obtained, while Stage III is the post-peak stage within the residual strain region. As mentioned above, each stage has its own controlling parameters. The governing equation for permeability evolution in the elastic range (Eq. (4)) is applied to fit the permeability data in the pre-peak stage (Stage I). The governing equation of permeability evolution in the damage phase (Eq. (16)) is applied to fit the permeability data in the post-peak stage (Stage II and Stage III) and the damage parameter (D) is calculated based on Eq. (15). The least square method is applied and the parameters used for the fitting curve are displayed in Table 1. During the fitting process we find that a changing γ instead of a constant γ can obtain good fits for Stages II and III. The Goodness of Fit (Regression coefficient, R^2) is used to illustrate the efficiency of the fitting results and its expression is written as:

$$R^2 = 1 - \frac{\sum (y_i - Y_i)^2}{\sum (y_i - y_{avg})^2} \quad (18)$$

in which y_i is measured permeability, y_{avg} is the average value of the permeability data and Y_i is the fitting value of the permeability data.

Shown as the regression coefficient values (R^2) in Table 1, the good fitting results are obtained especially when gas pressure is 2 MPa. In the original work, Xue et al. proposed a stress-dependent permeability model to fit the experiment data⁴²:

$$k = k_0 \times \left[\gamma \left(D - D_0 \right) + 1 \right] \times \exp \left\{ 3 \left(\frac{1}{K} - \frac{1}{K_p} \right) \left[\left(\sigma - \sigma_0 \right) - \left(p - p_0 \right) \right] \right\} \quad (19)$$

in which K_p is the modulus of pores, K is the modulus of the coal, and p is the gas pressure. The fitting results conducted by Xue et al. are also shown in Fig. 4 as the green line. As shown in the figure, two permeability values may be obtained at a single mean stress in Xue's model when the coal is damaged. While in our work, one strain value is associated with a unique permeability magnitude.

5. The topographic geological model and numerical model

In this section, the verified permeability model is applied to investigate co-exploitation of the coal seam and the uranium deposit. We select the strata distribution of the Dongsheng area, located in the northern part of Ordos Basin, China as the benchmark geologic conditions. The permeability variations under different mining approaches are investigated to assess the feasibility of the co-exploitation of the coal seam and uranium deposit.

5.1. Multi-resource Co-existence in the Ordos Basin, China

The Ordos Basin is located in north China, surrounded by the Yinshan Mountains to the north, the Qinling Mountains to the south, the Helan Mountains and Liupan Mountains to the west, and the Taihang Mountains to the east. It is the second largest inland sedimentary basin in China which is also encompassed by the Yellow River from its eastern, northern and western sides.⁵⁷ The structural framework of the basin is a large asymmetric syncline that dips gently 0.5–1.0 toward the east and north, and it has a slightly steeper dip angle of 2–3 toward the west and south.⁵⁸

More than fifty types of resources are found in the basin among which the coal, gas and sandstone-hosted uranium are essential for national strategic development. The proven coal and gas reserves are 213.3 billion tons and 1789.3 billion cubic meters, respectively, accounting for 13.7% and 17.3% of the national reserve. The general burial depth for oil and gas surpasses 1500 m, while coal resources have a depth less than 1000 m. Uranium was deposited in the Zhiluo Formation of the Middle Jurassic and Lower Cretaceous with a general burial depth ranging from 550 to 750 m. The primary distribution areas are the Haggin Banner, Ejin Horo Banner, Dongsheng area, and Etuokeqian Banner.

5.2. Coal seam and uranium deposit Co-existence conditions

A large uranium metallogenic belt has already been found in the Dongsheng area in the northern part of Ordos Basin, China. The Dongsheng area is one of the three largest coal fields in China. The Tarangaole coal minefield is located at the north part of Ordos Basin and serves as the first coal mine with ten-million-ton annual coal production in the Shenhua Group. The measured minable coal seams are 3-1, 4-1, 4-2, and 5-1, and the total coal reserves are 1.556 billion tons. The eastern region of this coal field is the Nalinggou uranium mine with an area of 32.86 km². The average burial depth of the uranium is 410 m, and the distances to the roof of coal seam 3-1, to the roof of the Jurassic confined aquifer, to the floor of the Jurassic confined aquifer, and to the floor of the Cretaceous confined aquifer are 90–150 m, 13–54 m, 80–147 m, and 210 m, respectively. The strata distribution of co-existing coal and uranium deposits is shown in Fig. 5.

5.3. Numerical model

The software COMSOL Multiphysics (Version 5.4) is used for the numerical investigation of co-exploitation of the coal seam and uranium deposits. The elastic-damage model and Mohr-Coulomb criterion were used to determine the stress-strain state, and the permeability model mentioned above is applied to investigate the permeability evolution during the coal mining activity. The geometric model is established based on the geological condition of Tarangaole coal mine. The strata are assumed horizontal as the dip angle of coal seam is shallow. For simplification, only the lower part of strata is simulated, and the effect of the upper part is treated as a formation stress with a magnitude of 10 MPa (based on the burial depth). The self-weight is also calculated. For the boundary condition, a uniaxial condition is established: the base of the model is a fixed constraint and the other sides were fixed in the direction normal to the faces. In this approach, the in-situ horizontal

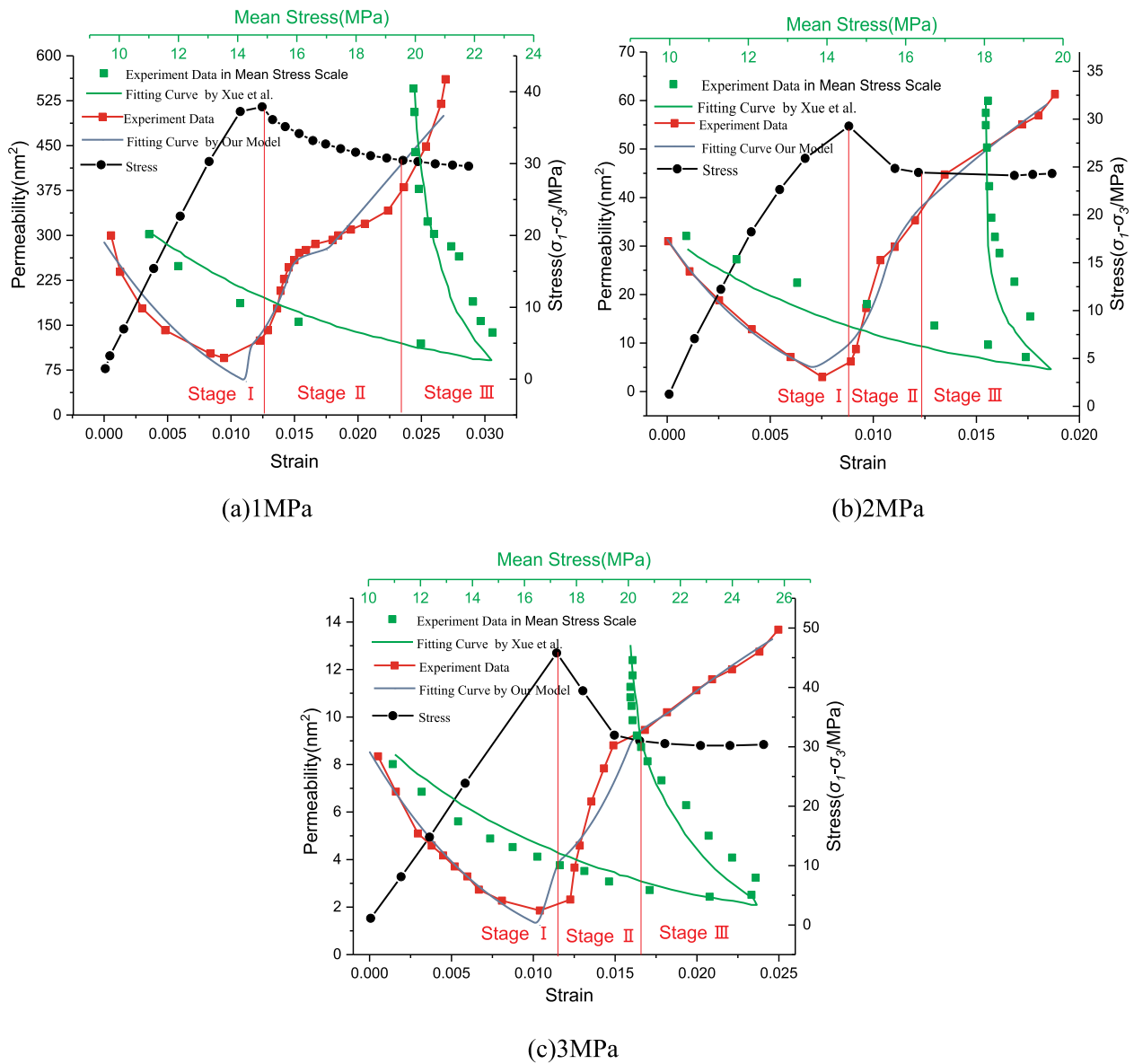


Fig. 4. Experimental results and fitting curves with different gas pressures.⁴² It should be noted that in Xue's work, the permeability is fitted in mean stress scale and the x-axis is in the top part of figure.

Table 1
Simulation parameters for model verification.

Gas Pressure	Stage I		Stage II		Stage III		R^2	
	k_0	α in Eq. (4)	ϕ_0 in Eq. (4)	γ in Eq. (16)	ε_{c0} in Eq. (15)	γ in Eq. (16)		λ_c in Eq. (15)
1 MPa	19.26	0.97	0.027	8.75	0.012	3.06	0.8	0.93
2 MPa	31.42	0.98	0.015	15	0.009	4.25	0.3	0.98
3 MPa	8.536	0.98	0.022	6.77	0.011	3	0.39	0.97

stress is calculated. This approach is also adopted by other researchers²⁴ and the application library of COMSOL Multiphysics.⁶⁰ Coal seam 3-1 is selected as the minable seam and the mining area is located 100m–300 m along the horizontal direction from left to right. The strata above the coal seam are mainly sandstone therefore in this work only the coal seam and sandstone are considered. The interface between the two domains are not treated in any special way other than that the strain and stress on the interface between the two domains are

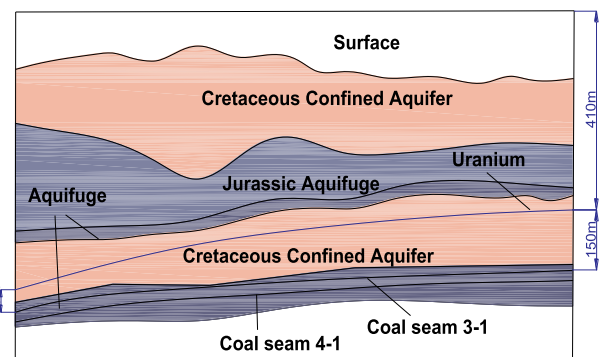


Fig. 5. Schematic of the co-existing coal and uranium deposits in the Tarangaole mine area in the Ordos Basin⁵⁹

continuous. The numerical model is shown in Fig. 6 based on the strata distribution shown in Fig. 5 and the parameter values shown in Table 2, collected from the literature.^{34,61}

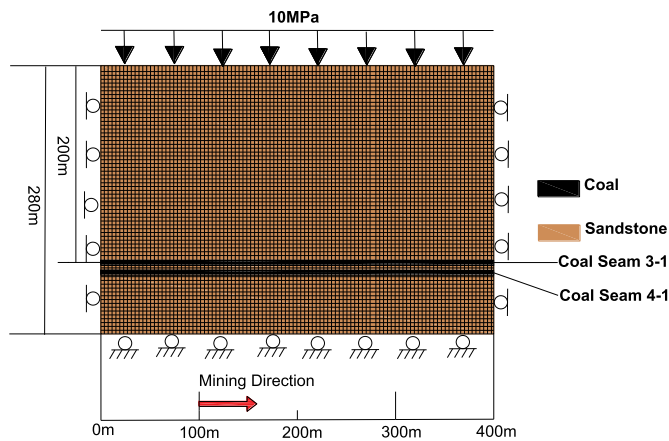


Fig. 6. The illustration of the numerical model.

The numerical model follows the rock deformation and implements the damage criterion. The deformation of the rock is calculated using the Solid Deformation module of COMSOL Multiphysics, and the damage criterion is determined from Eq. (12) and checked with the MATLAB. Once the criterion is satisfied, the reduced Young's modulus is calculated based on Eqs. (13)–(15). Then the calculated Young's modulus is returned to COMSOL Multiphysics for the calculation of the next step. This iteration process is carried out through COMSOL coupled with MATLAB, a commercial software to connect COMSOL Multiphysics to the MATLAB scripting environment.⁶²

5.4. Parametric study

We designed three scenarios based on this geological model as shown in Table 3. These scenarios are: (i) regular longwall mining, (ii) coal room-and-pillar mining and (iii) coal top-caving mining. Scenario (i) is used as the benchmark model and compared with the empirical equation. Scenario (ii) has two sub-cases representing a single coal pillar located at 180–220 m (sub-case(a)), and two coal pillars located at 160–180 m and 240–260 m (sub-case(b)). The mining areas of the two sub-cases in Scenario (ii) are identical. The mining height is 4 m in Scenario (iii). The mining areas of Scenarios (ii) and (iii) are also the same. The details of the three cases are illustrated in Table 3 and the results are reported in the following sections.

6. Results and discussion

6.1. The results of benchmark model

The results of the benchmark model (Scenario (i)) are first reported and compared with the empirical equations to verify the applicability of the model.

6.1.1. Damage evolution of the coal mining area

When the coal seam is exploited, the rock mass around coal seam experiences damage and deformation including roof fall and floor heave as shown in Fig. 7. In this damage region, the resulting fractures provide flow channels for gas and other fluids. As shown in the figure, the damage zone evolves with mining advance. When mining advance was 40 m, a rectangular-shaped damage zone forms over the roof of the coal

seam with a length of 20 m and a height of 4 m. With the continuation of the coal seam mining, the damage zone gradually expands. When the mining advance was 200 m, a trapezoid shaped damage zone above the roof is formed with a length of 160 m and a height of 21 m. In that situation, a large number of fractures form and eventually link-up forming a channel for water or other fluids to the gob and working face. The shape and size of the damage zone are similar with that shown by Kong et al.²⁴

6.1.2. Redistribution of stress

During the mining process, the stress is redistributed. In this section, we analyze the variations of the horizontal stress and vertical stress with the coal mining process at a height of 5 m above the coal seam at different mining advances. We select mining advances of 20 m, 80 m, 120 m, 160 m, and 200 m and show the horizontal and vertical stresses in Fig. 8. As shown in the figure, stress will increase at the coal face as an abutment stress²¹ and it will compress and break the coal and rock mass. Fig. 8 also shows that the peak value of the abutment stress gradually increases with mining advance. Comparing Fig. 8 (a) and (b), we find that the horizontal-stress and vertical-stress have different changes. The vertical stress peak is in compression at the abutment and is zero interior to panel edges – this is due to the boundary condition of zero vertical stress on the panel roof and floor. The vertical stress decays to background vertical stress away from the panel. The horizontal stress approaches zero at the panel edge (since it is 5 m above the panel) and is in tension over the panel due to the sagging of the panel floor and roof. The horizontal stress approaches the regional horizontal stress remote from the panel. Finally, the inflection of the horizontal stress within the panel and towards the panel edge, is where the trajectory of the measuring line transits the shear lobes at the panel edge that are present symmetrically both above and below the panel. These are standard results and this phenomenon is also confirmed by Yang et al.²¹

In this section, seven reference lines above the goaf (5 m, 20 m, 40 m, 60 m, 80 m, 100 m and 140 m) are selected to investigate the variations of the stresses, with the results are shown in Fig. 9. The vertical stresses on the seven reference lines all decrease over the mining area (100m–300 m) as shown in Fig. 9 (b). The vertical stress returns to the in-situ stress gradually as the distance to the mining area becomes larger. Also, the shorter the distance to the coal seam, the larger the reduction in vertical stress. The redistribution of the horizontal stress over the reference lines are more complicated than that of vertical stress as shown in Fig. 9 (a). The evolution of horizontal stress exhibits two opposing trends: the stress is lower than the original stress when the distance to the goaf is within 60 m and the horizontal stress is released; but the stress will be higher than the original value beyond this distance serving as a compression stress.

6.1.3. Comparison of numerical and empirical results

In this section, the numerical results of the benchmarked model are compared with the results obtained from empirical equations. For flat or nearly flat seams subject to longwall mining, the average height of the caved roof can be determined by the following equation^{11,63}:

$$H_c = \frac{100h}{c_1h + c_2} \quad (20)$$

where H_c is the caved zone height; h is the mining height, and c_1 and c_2 are coefficients depending on strata lithology as shown in Table 4. Also

Table 2
Simulation parameters for coal and uranium co-exploitation.^{34,61}

Strata	Density (kg/m ³)	Young's Modulus (GPa)	Friction Angle (°)	Cohesion (MPa)	Uniaxial Tensile Stress (MPa)	Uniaxial Compressive Stress (MPa)
Coal	1300	8	16	8	2	20
Sandstone	2500	28	28	10	5	48

Table 3
Scenarios of numerical modeling for co-exploitation of coal and uranium.

Scenario	Mining Area(m ²)	Mining Height(m)	Pillar location
i longwall mining	1000	5	–
ii room-and-pillar mining			–
a one pillar	800	5	180–220 m
b two pillar	800	5	160–180 m, 240–260 m
iii top caving mining	800	4	–

the following equation can be used for the estimation of the average height of the fractured zone^{11,63}:

$$H_f = \frac{100h}{c_3h + c_4} \quad (21)$$

where H_f is the fracture zone height; h is the mining height, and c_3 and c_4 are coefficients depending on strata lithology as shown in Table 4.

Based on Eqs. (20) and (21), and the parameters shown in Table 4, the heights of the caved and fractured zones are 19 m and 62.5 m, respectively. As illustrated above, a trapezoidal shape of the damage zone above the roof would be formed and its height (21 m) is almost equal to the height of the caved zone (19 m). From this perspective, the variation in size of the damage zone can partly represent the evolution of the caved zone. Also as shown in Fig. 1, in both caved and fractured zones the horizontal stresses are reduced while in the constrained zone the horizontal stress is larger than the original value, serving as an effective compressive stress. Based on our numerical results (Fig. 9 (a)), the horizontal stress is larger than the original value at the reference line at 60 m (the absolute value is used here). Below 60 m, the horizontal stress is destressed. We can conclude that the height of fractured zone penetrates approximately 60 m into the mining area which corresponds closely with the empirical equation (62.5 m).

To verify our model applicability, the evolution of the damaged zone is compared with the work of Kong et al.²⁴ and the heights of the caved and fractured zones are compared with various empirical equations^{11,63} – all with satisfactory fits. The comparison of results demonstrates that our proposed model can accurately predict stratum movement after coal mining even though the interface between the two domains is not specially treated.

6.1.4. Investigation of permeability anisotropy

The redistributions of permeabilities in the horizontal direction and vertical direction on the six reference lines above the goaf (5 m, 20 m, 40 m, 60 m, 100 m, and 140 m) are both illustrated in Fig. 10. We also compared the difference of permeability values both with and without considering the effect of damage.

As illustrated above, the height of the damage zone is ~21 m high above the goaf. As shown in Fig. 10, the calculated permeability value, considering the damage effect, is much higher than that ignoring the damage effect. The incremental ratios of the horizontal and vertical permeability are assumed equivalent in the damage zone. Apart from the damage zone, the value of horizontal permeability changes significantly as the largest value is ~300 times that of the initial value, while for the vertical permeability the value is only ~110 times. Generally, the incremental ratios of both horizontal and vertical permeabilities decrease when the distance to the goaf becomes larger. The horizontal permeability near the working face is larger than the value in the core of the caved zone because of vertical compression. The vertical permeability is larger than the initial value on the rib area adjacent to the goaf area.

Compared to Fig. 1, we observe that in both caved and fractured zones, the horizontal and vertical permeabilities are larger than the initial value especially in the damage zone. While in the constrained zone, the horizontal permeability is larger than the initial value and the vertical permeability retains its original value.

6.2. The results of coal room-and-pillar mining method

6.2.1. Damage evolution in the coal mining area

In the second scenario, we simulate the mining process with the room-and-pillar mining. Two sub-cases are designed: for sub-case (a) one pillar is left in the location 180–220 m; for sub-case (b) two pillars are left at locations 160–180 m and 240–260 m with the mining areas of the two sub-cases identical. We first illustrate the damage zone evolution under the two sub-cases, with the results shown in Fig. 11.

Similar to the results of the benchmark model, a trapezoidally shaped damage zone also exists above the mining area. Compared with Fig. 7, the heights of the trapezoidal damage zone obtained from the room-and-pillar approach are much smaller than that obtained from the benchmark model representing regular longwall mining. Comparing Fig. 11(a) and (b), the height of the damaged trapezoid of sub-case (a) is larger than that of sub-case (b).

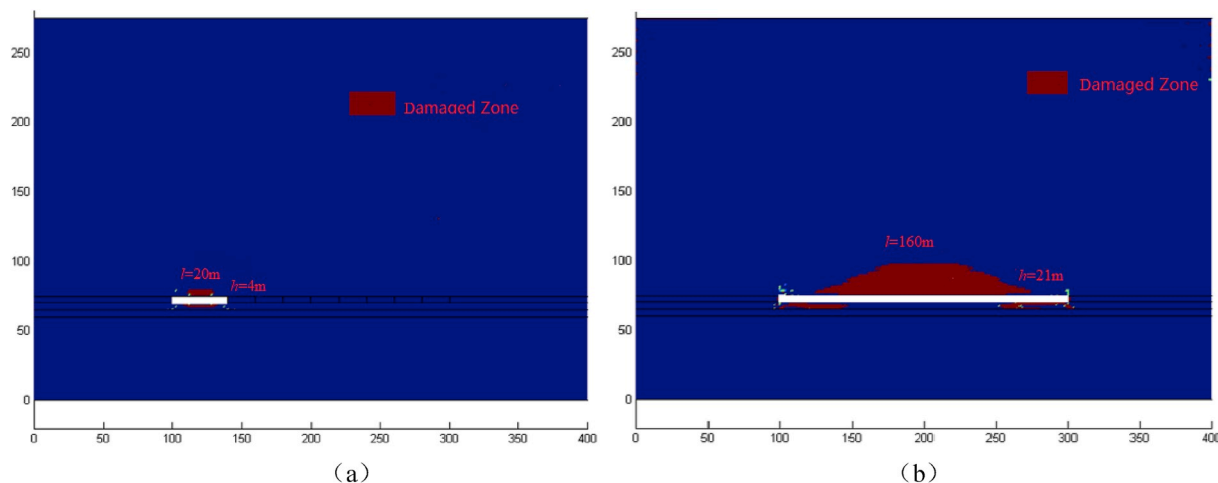


Fig. 7. Damage zone evolution of Scenario (i) at mining distances of (a) 40 m and (b) 200 m.

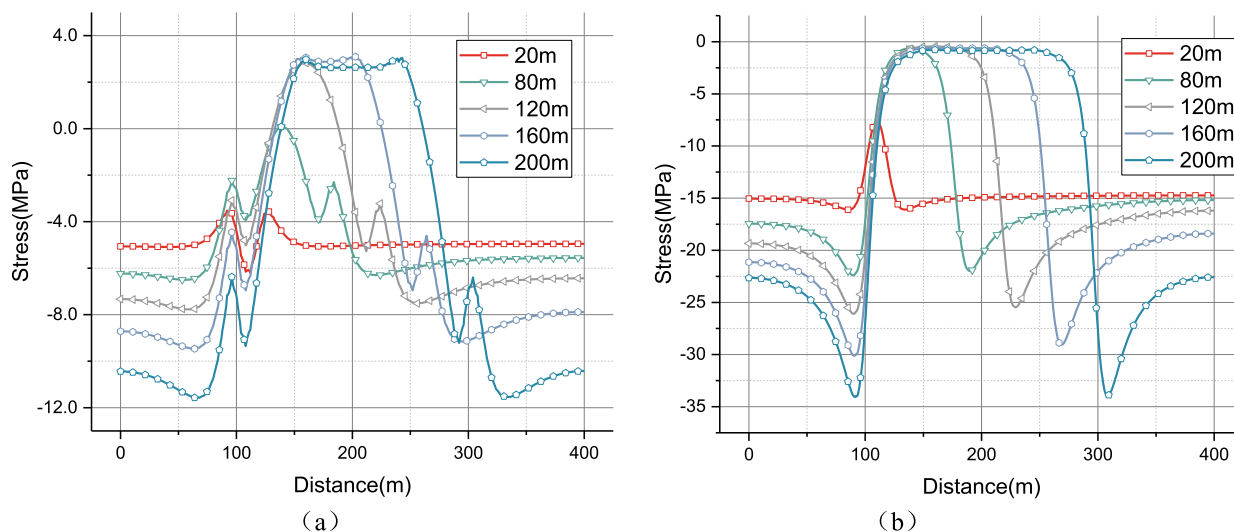


Fig. 8. Redistribution of (a) horizontal stress; and (b) vertical stress at different mining advances 5 m above the panel.

6.2.2. Investigation of permeability anisotropy

We also illustrate the permeability evolution of sub-case (a) and sub-case (b) with the results displayed in Figs. 12 and 13, respectively. The coal pillar separates the coal into several coal mining areas, and the evolution of both the horizontal and vertical permeability above each mining area are similar to the results under longwall mining. The most significant difference is that there will be a permeability enhancement area for the horizontal permeability between the two mining areas. The variation rate (k/k_0) is much smaller in both directions under both sub-cases compared with the results for regular longwall mining. Comparing Figs. 12 with 13, we find that the permeability increment ratio of the sub-case (a) is larger than that of sub-case (b) in the damaged zones. In the undamaged zone, the horizontal permeability increment ratio of sub-case (a) is larger than that of sub-case (b) while for the vertical permeability the opposite situation is observed in the above region between the two mining areas.

6.3. Results for top-caving mining

6.3.1. Damage evolution in the coal mining area

The evolution of the damage zone under the scenario of top-caving is illustrated in Fig. 14. Similar to the results for longwall mining, a

trapezoid shaped damage zone appears above the goaf with its size expanding with mining advance. Compared with Fig. 7, we find that the size of the damage zone under the case of top-caving is similar to that of regular longwall mining. As shown in the figure, the length of the damage zone is almost the same as the benchmark model although the height of the trapezoid zone is smaller than that resulting from regular longwall mining.

6.3.2. Investigation of permeability anisotropy

Permeability evolution under the scenario of top-caving mining is similar to the first case of the benchmark model as shown in Fig. 15 with the variation rate (k/k_0) smaller in both directions compared with the first scenario of longwall mining. Taking the variation rate of horizontal permeability (k_h/k_{h0}) as an example, the largest variation ratios in both the elastic and damage zones are each ~ 250 while the value of the first scenario is ~ 300 that in the elastic zone and 350 in the damage zone. It can be concluded that top-caving can reduce the area of the damage zone and cause less disturbance on the overlying strata.

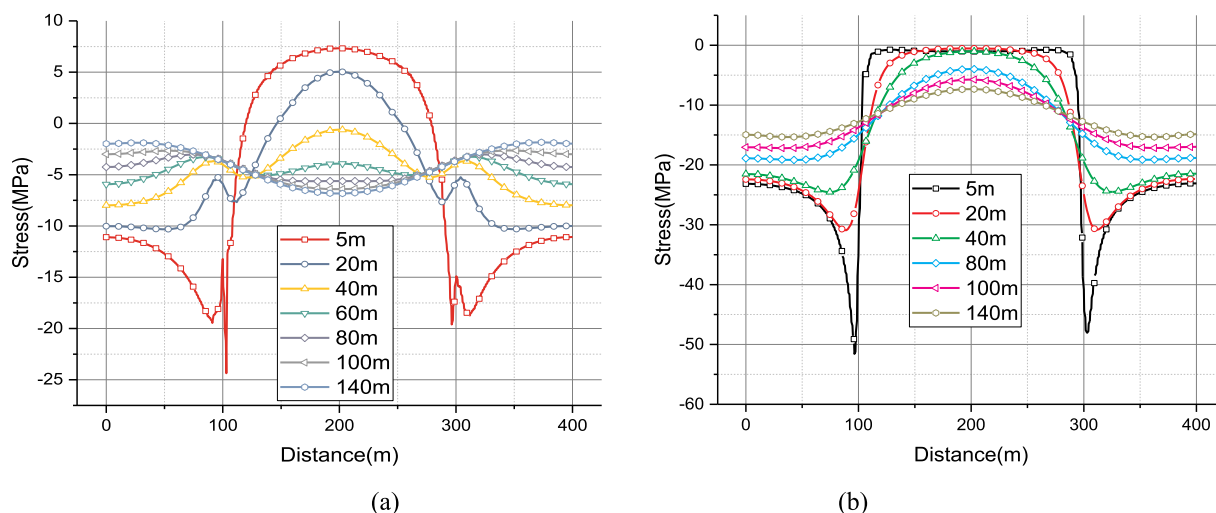


Fig. 9. The redistribution (a) horizontal stress and (b) vertical stress at the different distance to the goaf.

Table 4
Strata lithology parameters for the calculation of caved zone and fracture zone height.^{11,63}

Strata Lithology	Compressive Strength (σ_c , MPa)	Coefficients	
		c_1 and c_3	c_2 and c_4
Strong and hard	> 40	2.1 for caved zone 1.2 for fractured zone	16 for caved zone 2 for fractured zone
Medium strong	20–40	4.7 for caved zone 1.6 for fractured zone	19 for caved zone 3.6 for fractured zone
Soft and weak	< 20	6.2 for caved zone 3.1 for fractured zone	32 for caved zone 5 for fractured zone

6.4. Discussion of coal and uranium Co-exploitation

6.4.1. Co-exploitation patterns of coal and uranium

Underground mining is widely applied to coal recovery in China. If the same technology is applied to uranium resources, no more than one ton of uranium can be extracted when 1000 tons of ore is excavated underground, as the average uranium-bearing ore grade of China is about 0.1%. Meanwhile, 3000 tons of waste water is produced. Considering these disadvantages, leaching is typically applied to uranium resource recovery with a neutral solution used composed of CO_2 , O_2 , and water. Unlike underground mining, the leaching does not induce significant strata deformation and the solid waste is only stored in instruments, equipment, and pipes which are easily collected. Leaching includes the following steps in sequence⁵⁹: first, the leaching solution is injected into the uranium strata through a borehole and a chemical reaction is initiated between the leaching solution and the components in the strata. Then the valuable components in the uranium deposit are dissolved and a uranium-bearing leaching solution is formed. Finally, the uranium-bearing leaching solution is extracted to the surface through a liquid-extraction borehole.

Water is required for leaching, whereas water must be drawn off for the coal mining. In addition to this, uranium is a radioactive element and a possible leak will critically damage flora and fauna and endanger personnel.^{4,5} Thus, improper co-exploitation of coal and uranium may result in significant environmental and health problems. As analyzed above, four zones are formed after coal mining, as defined with characteristic permeability structure. If the uranium is close to the coal seam and located in the areas of the caved and fractured zones, the coal mining would induce a large strata movement and the leaching solution would leak, threatening the workers and the mining operation. Under this situation, a coal seam beneath the uranium deposit should be abandoned. Conversely, if the uranium is located in the area of the

constrained zone, the horizontal permeability increases due to coal mining but the vertical permeability may maintain its initial value. Under this situation, coal mining would be helpful to the uranium exploitation as the increased horizontal permeability would enhance the transport of the leaching solution. While some sealing technology could be applied to the coal panel roof as the vertical permeability in the rib area of constrained zone would increase.

6.4.2. The influence of the mining approach

As discussed above, the zone in which the uranium deposit would reside following coal mining plays a significant role for the co-exploitation of the coal and uranium deposits. The division into the above four zones and the related permeability variations vary with the different mining approaches. To fully illustrate this, we compared the size of the damaged zone (caved zone) and the maximum permeability ratio along the two reference lines (20 m and 40 m) above the goaf for the different mining approaches with the comparison results shown in Table 5. We first compare the results obtained from room-and-pillar mining approach with longwall mining. As illustrated in the table, the room-and-pillar mining approach can significant decrease the size of damage zone. Both the horizontal and vertical permeability ratios at 20 m above the coal mining area are significantly decreased. The permeability variations on the reference line at 40 m are different: the horizontal permeability ratio is sharply decreased, and the vertical permeability decreases for the case of two pillars but increases for the case of one pillar. While the maximum vertical permeability ratio on the reference line at 40 m appears on the location between the two mining areas rather the area directly above the goaf. For the top-caving mining approach, both the damaged zone and permeability ratios at both reference lines are slightly decreased compared with the results of regular longwall mining.

As discussed above, the best location for the uranium deposit is the

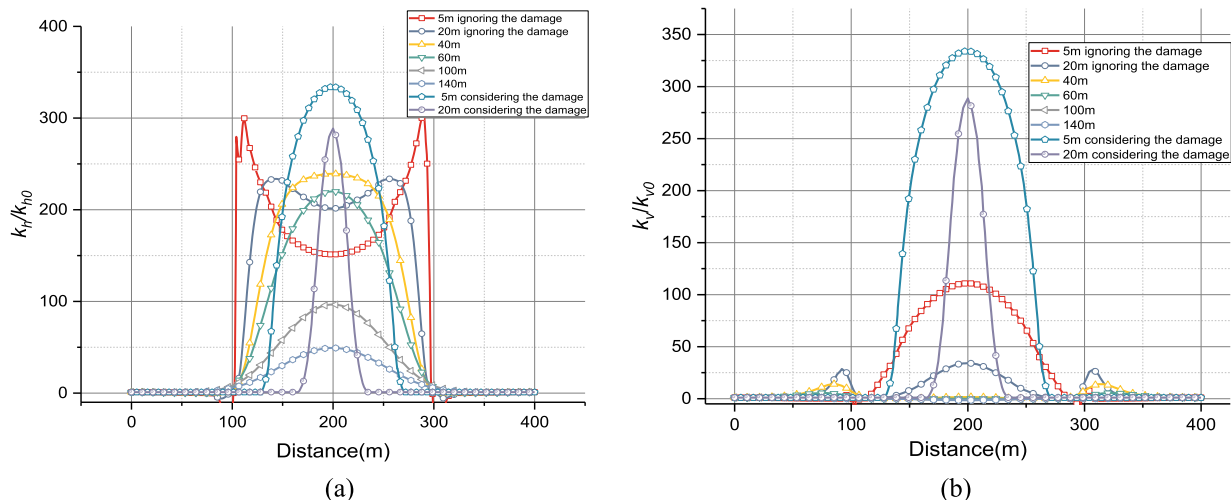


Fig. 10. Variation of permeability (a) horizontal and (b) vertical.

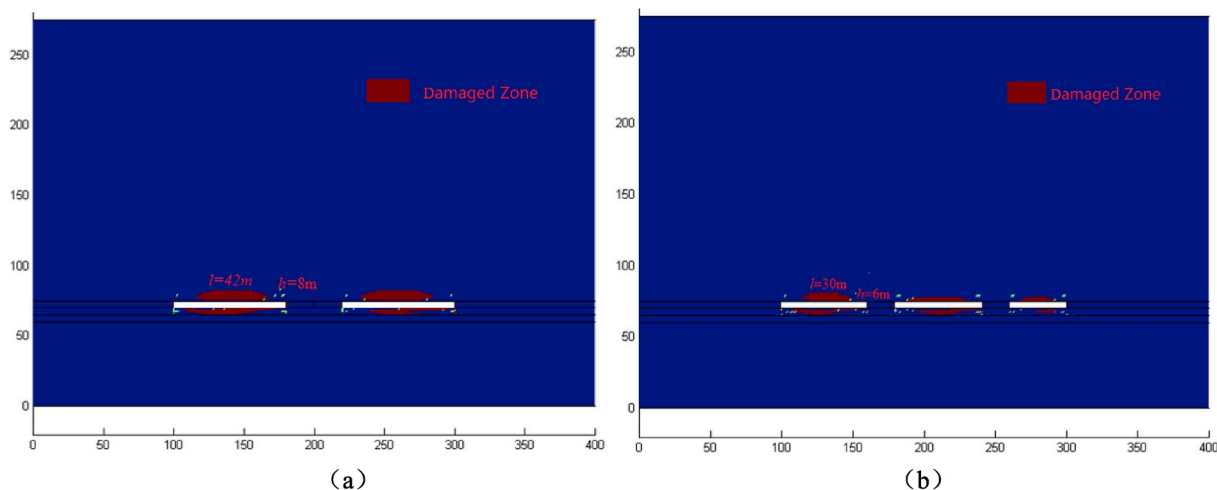


Fig. 11. Damage evolution of the coal pillar mining approach after the exploitation of (a) with one pillar and (b) with two pillars removed.

constrained zone following coal mining as in this zone the increased horizontal permeability would enhance the flow of the leaching solution in the uranium deposit and the invariant vertical permeability would contain the leaching solution in the uranium deposit. The distance between the constrained zone and the coal mining area can be adjusted by the mining approach. If the distance between coal seam and the uranium deposit is very large, then the uranium deposit is located at the surface zone or constrained zone after coal mining. The regular longwall mining approach can be applied in that situation. If the distance between the uranium deposit and coal seam is small then the uranium deposit would be located in fractured zone after the coal mining. The regular longwall mining approach should be abandoned. In that situation, the room-and-pillar mining approach or the top caving mining approach should be applied. As shown in the simulation results, both approaches would reduce the disturbance of the coal mining to the zone above uranium deposit and decrease the maximum permeability ratio. While the permeability variations are different under top-caving and room-and-pillar mining approaches, the top caving approach can slightly decrease the permeability ratio and can be applied when the uranium deposit is located at the interface between fractured zone and constrained zone. Conversely, room-and-pillar mining can significantly decrease the permeability ratio and significantly shorten the length of fractured zone. However when the room-and-pillar mining approach is applied, sealing technology should be applied to the coal roof as the

vertical permeability between the coal pillars would increase. If the uranium deposit is located very close to the coal seam, such as in the caved zone, the coal seam should be abandoned for safety and environmental reasons.

7. Conclusions

In this work, a novel strain-dependent permeability model is proposed to investigate the feasibility of co-exploitation of coal seam and uranium deposits. First, experimental data collected from a stress-strain-permeability test are used for model verification. Then a numerical model based on the geologic conditions of the Dongsheng area in the northern part of Ordos Basin, China is established, and three recovery scenarios are explored. The influences of mining approaches on the co-exploitation of coal seam and uranium deposit are discussed. Based on the model verification and simulation results, the following conclusions are drawn:

- (a) In this work, a strain-dependent permeability model is proposed in which the permeability evolution is related to the effective strain in the elastic range and associated with the damage parameter (D) when coal is damaged. The proposed model is applied to curve-fit the experimental data recovered from a stress-strain-permeability test with good fitting results. A single strain value is associated with

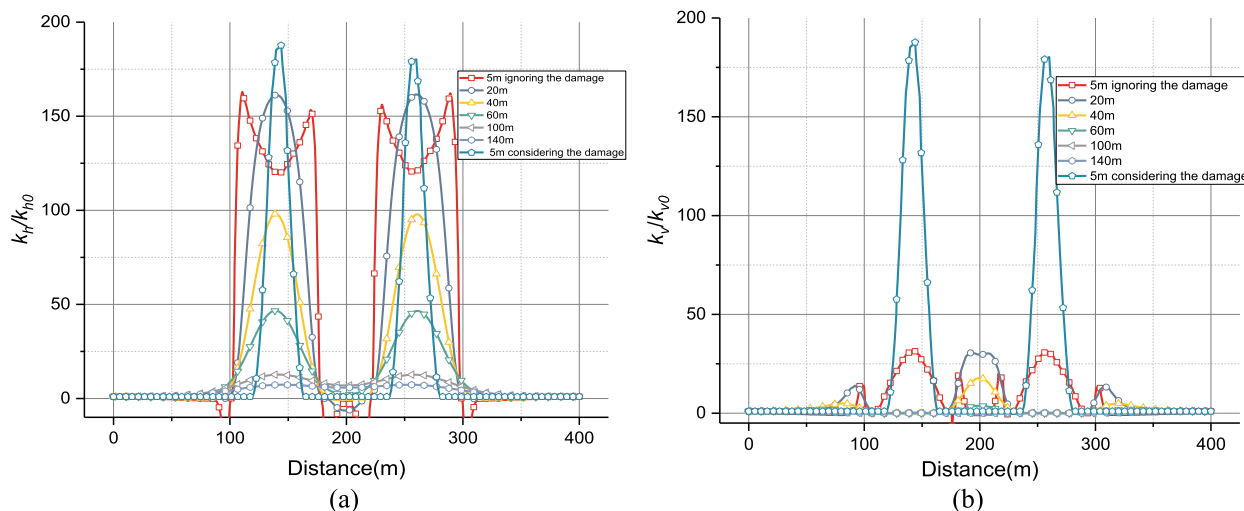


Fig. 12. Variation in permeability of Scenario(ii) with one pillar for (a) horizontal and (b) vertical permeability.

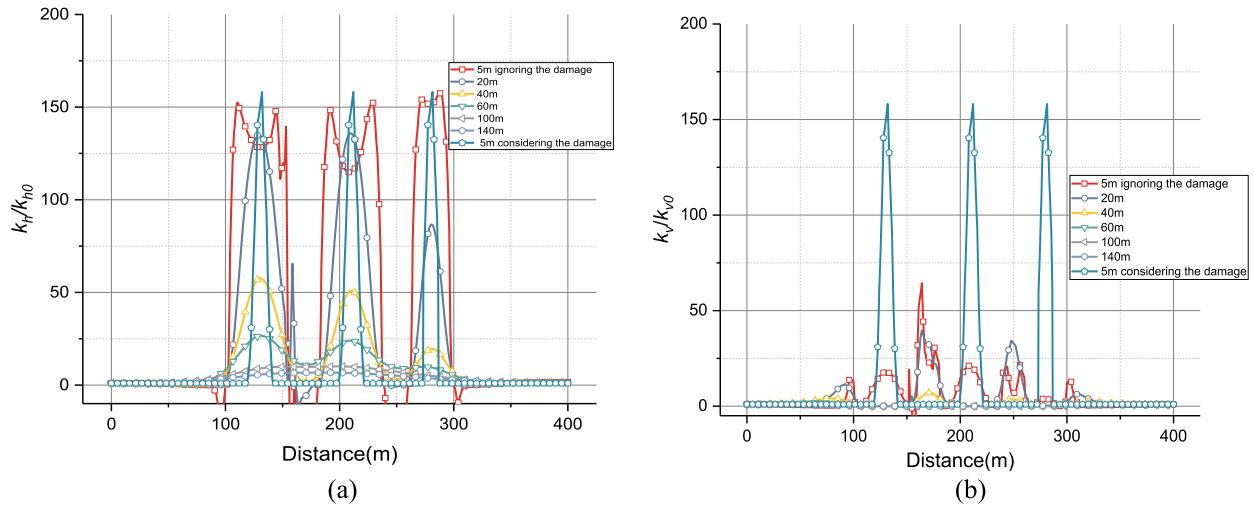


Fig. 13. Variation of permeability of Scenario (ii) with two pillars for (a) horizontal and (b) vertical permeability.

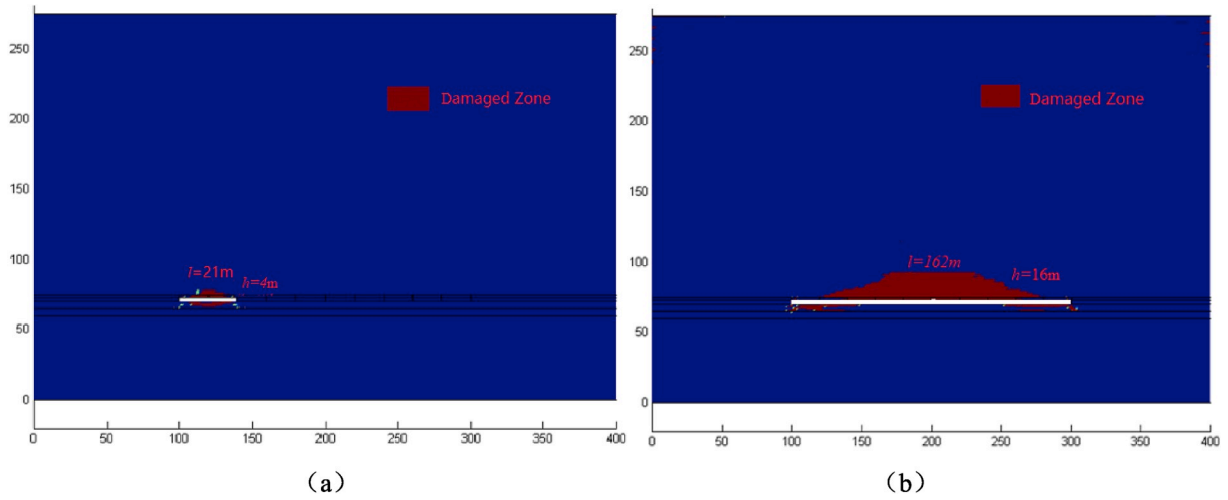


Fig. 14. Damage evolution for scenario (iii) with mining advances of (a) 40m and (b) 200m under the scenario of top caving.

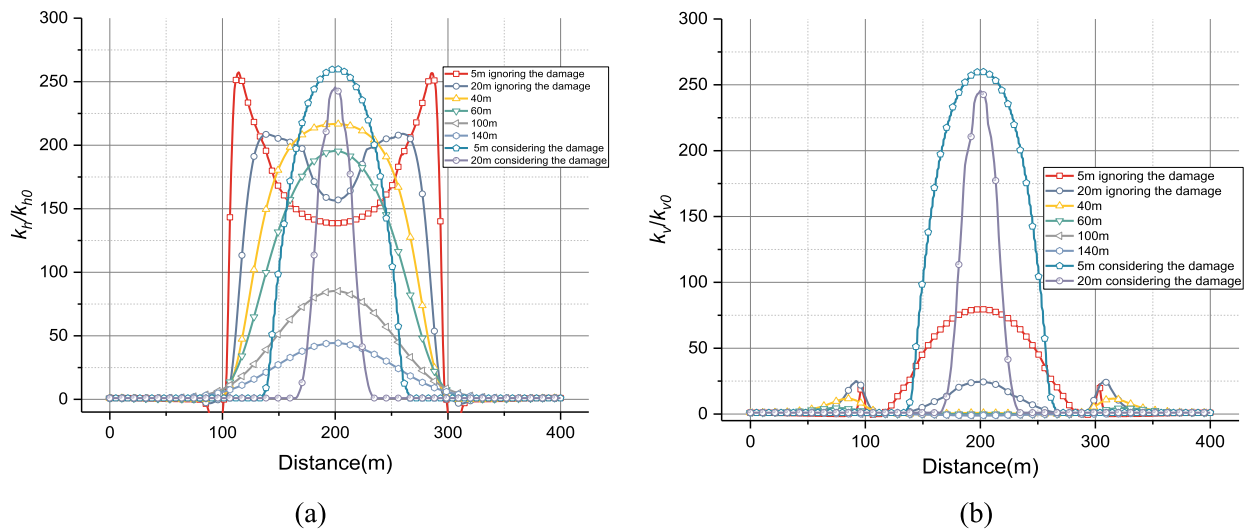


Fig. 15. Variation in (a) horizontal and (b) vertical permeability due to top-caving.

Table 5
Comparisons of damaged zone and maximum permeability ratio with different mining approaches.

Scenario	Size of Damaged Zone		Maximum Permeability Ratio at 20 m		Maximum Permeability Ratio at 40 m	
	Length	Height	Horizontal(k_h/k_{h0})	Vertical(k_v/k_{v0})	Horizontal(k_h/k_{h0})	Vertical(k_v/k_{v0})
i longwall mining	160 m	21 m	288	288	240	15
ii room-and-pillar						
a one pillar	42 m	8 m	160	32	96	17
b two pillar	30 m	6 m	130	40	55	8
iii top caving	162 m	16 m	240	240	218	13

- a unique permeability in our new model while in the stress-dependent permeability model duplicate permeability values may be obtained for a single mean stress value when the coal is damaged.
- (b) After coal mining the strata above the goaf can be divided into four zones in which the uranium deposit could reside after coal mining plays a significant role for the feasible co-exploitation of the coal seam and uranium deposit. When the uranium deposit lays in the caved or fractured zones, the leaching solution would leak into the coal seam and the coal seam under the uranium deposit would have to be abandoned. When the uranium deposit lays in the constrained zone, the enhanced horizontal permeability value would enhance the flow of the leaching solution in the uranium deposit and the coal seam mining would be a benefit to the uranium deposit exploitation. When the uranium deposit lays in the surface zone, the exploitation of the two resources has almost no effect on each other.
- (c) The locations of the four zones can be modified by the selected mining approach. Longwall mining results in the largest disturbance to the overlaying strata and the most extensive caved and fractured zones followed by the top caving mining approach then the room-and-pillar mining approach. If the uranium deposit is located at the interface between the fractured and constrained zones, top-caving mining should be applied to ensure that the uranium deposit is located in the constrained zone. If the uranium deposit is located in the fractured zone but near the constrained zone, then the room-and-pillar mining approach should be applied. Meanwhile sealing technology could be applied especially to the areas above coal pillars to contain fluids migration and ensure safe operation.

Acknowledgments

The research delivered partial results under supports of the Natural Science Foundation of China (51609038), the 111 Project (B17009) and the Fundamental Research Funds for the Central Universities (No. N160104002).

Appendix A. Supplementary data

Supplementary data to this article can be found online at <https://doi.org/10.1016/j.ijrmms.2019.104098>.

References

- Dai S, Yang J, Ward CR, et al. Geochemical and mineralogical evidence for a coal-hosted uranium deposit in the Yili Basin, Xinjiang, northwestern China. *Ore Geol Rev*. 2015;70:1–30.
- Zhang L, Liu C, Lei K. Green altered sandstone related to hydrocarbon migration from the uranium deposits in the northern Ordos Basin, China. *Ore Geol Rev*. 2019;109:482–493.
- Fuchs S, Schumann D, Williams-Jones AE, Vali H. The growth and concentration of uranium and titanium minerals in hydrocarbons of the Carbon Leader Reef, Witwatersrand Supergroup, South Africa. *Chem Geol*. 2015;393–394:55–66.
- Tewari R, Horemans N, Nauts R, Wannijn J, Van Hees M, Vandenhove H. Uranium exposure induces nitric oxide and hydrogen peroxide generation in *Arabidopsis thaliana*. *Environ Exp Bot*. 2015;120:55–64.
- Atkins ML, Santos IR, Perkins A, Maher DT. Dissolved radon and uranium in groundwater in a potential coal seam gas development region (Richmond River Catchment, Australia). *J Environ Radioact*. 2016;154:83–92.
- Bister S, Birkhan J, Lüllau T, et al. Impact of former uranium mining activities on the

- floodplains of the Mulde River, Saxony, Germany. *J Environ Radioact*. 2015;144:21–31.
- Baborowski M, Bozau E. Impact of former mining activities on the uranium distribution in the River Saale (Germany). *Appl Geochem*. 2006;21(6):1073–1082.
 - Rongxi L, Youzhu L. The geologic features of mineralization at the Dongsheng uranium deposit in the northern Ordos Basin (Central China). *Russ Geol Geophys*. 2011;52(6):593–602.
 - Yuan L, Zhang T, Zhao Y, Ren B, Hao X, Xu C. Precise coordinated mining of coal and associated resources: a case of environmental coordinated mining of coal and associated rare metal in Ordos basin. *J China Inst Min Technol*. 2017;46(3):449–459.
 - Joksić A, Katz SA. Chelation therapy for treatment of systemic intoxication with uranium: a review. *Environ Lett*. 2015;50(14):1479–1488.
 - Yavuz H. An estimation method for cover pressure re-establishment distance and pressure distribution in the goaf of longwall coal mines. *Int J Rock Mech Min Sci*. 2004;41(2):193–205.
 - Gao F, Xue Y, Gao Y, Zhang Z, Teng T, Liang X. Fully coupled thermo-hydro-mechanical model for extraction of coal seam gas with slotted boreholes. *J Nat Gas Sci Eng*. 2016;31:226–235.
 - Forster I, Enever J. *Hydrogeological Response of Overburden Strata to Underground Mining, Central Coast, New South Wales: Appendices*. Office of Energy Report; 1992.
 - Adhikary DP, Guo H. Measurement of longwall mining induced strata permeability. *Geotech Geol Eng*. 2014;32(3):617–626.
 - Adhikary DP, Guo H. Modelling of longwall mining-induced strata permeability change. *Rock Mech Rock Eng*. 2015;48(1):345–359.
 - Zhang C, Tu S, Zhang L, Wang F, Bai Q-s, Tu H. The numerical simulation of permeability rules in protective seam mining. *Int J Oil Gas Coal Technol*. 2016;13(3):243–259.
 - Bai M, Elsworth D. Some aspects of mining under aquifers in China. *Min Sci Technol*. 1990;10(1):81–91.
 - Holla L, Buizen M. The ground movement, strata fracturing and changes in permeability due to deep longwall mining. *Int J Rock Mech Min*. 1991;28(2-3):207–217.
 - Booth CJ, Spande ED. Potentiometric and aquifer property changes above subsiding longwall mine panels, Illinois basin coalfield. *Gr Water*. 1992;30(3):362–368.
 - Majidi A, Hassani FP, Nasiri MY. Prediction of the height of distressed zone above the mined panel roof in longwall coal mining. *Int J Coal Geol*. 2012;98(1):62–72.
 - Yang W, Lin B, Qu Y, et al. Stress evolution with time and space during mining of a coal seam. *Int J Rock Mech Min Sci*. 2011;48(7):1145–1152.
 - Zhang R, Cheng Y, Zhou H, et al. New insights into the permeability-increasing area of overlying coal seams disturbed by the mining of coal. *J Nat Gas Sci Eng*. 2018;49:352–364.
 - Liu Y, Zhuo F, Lliu L, Liu C, Hu S. An experimental and numerical investigation on the deformation of overlying coal seams above double-seam extraction for controlling coal mine methane emissions. *Int J Coal Geol*. 2011;87(2):139–149.
 - Kong X, Wang E, Liu Q, et al. Dynamic permeability and porosity evolution of coal seam rich in CBM based on the flow-solid coupling theory. *J Nat Gas Sci Eng*. 2017;40:61–71.
 - Wang C, Liu J, Feng J, Wei M, Wang C, Jiang Y. Effects of gas diffusion from fractures to coal matrix on the evolution of coal strains: experimental observations. *Int J Coal Geol*. 2016;162:74–84.
 - Pan Z, Connell LD. A theoretical model for gas adsorption-induced coal swelling. *Int J Coal Geol*. 2007;69(4):243–252.
 - Seidle JP, Jeanson MW, Erickson DJ. Application of matchstick geometry to stress dependent permeability in coals. *SPE Rocky Mountain Regional Meeting*. Society of Petroleum Engineers; 1992.
 - McKee CR, Bumb AC, Koenig RA. Stress-dependent permeability and porosity of coal and other geologic formations. *SPE Form Eval*. 1988;3(1):81–92.
 - Chen T, Feng X-T, Cui G, Tan Y, Pan Z. Experimental study of permeability change of organic-rich gas shales under high effective stress. *J Nat Gas Sci Eng*. 2019;64:1–14.
 - Palmer I, Mansoori J. How permeability depends on stress and pore pressure in coalbeds: a new model. *SPE Annual Technical Conference and Exhibition*. Society of Petroleum Engineers; 1996.
 - Shi JQ, Durucan S. Drawdown induced changes in permeability of coalbeds: a new interpretation of the reservoir response to primary recovery. *Transp Porous Media*. 2004;56(1):1–16.
 - Peng Y, Liu J, Wei M, Pan Z, Connell L. Why coal permeability changes under free swellings: new insights. *Int J Coal Geol*. 2014;133:35–46.
 - Cui G, Liu J, Wei M, Shi R, Elsworth D. Why shale permeability changes under variable effective stresses: new insights. *Fuel*. 2018;213:55–71.
 - Yang W, Lin B, Qu Y, et al. Mechanism of strata deformation under protective seam and its application for relieved methane control. *Int J Coal Geol*. 2011;85(3-4):300–306.

35. Wang K, Zang J, Wang G, Zhou A. Anisotropic permeability evolution of coal with effective stress variation and gas sorption: model development and analysis. *Int J Coal Geol.* 2014;130:53–65.
36. An H, Wei XR, Wang GX, et al. Modeling anisotropic permeability of coal and its effects on CO₂ sequestration and enhanced coalbed methane recovery. *Int J Coal Geol.* 2015;152:15–24.
37. Wang S, Elsworth D, Liu J. Permeability evolution during progressive deformation of intact coal and implications for instability in underground coal seams. *Int J Rock Mech Min Sci.* 2013;58:34–45.
38. Souley M, Homand F, Pepa S, Hoxha D. Damage-induced permeability changes in granite: a case example at the URL in Canada. *Int J Rock Mech Min Sci.* 2001;38(2):297–310.
39. Shao J, Chau K, Feng X. Modeling of anisotropic damage and creep deformation in brittle rocks. *Int J Rock Mech Min Sci.* 2006;43(4):582–592.
40. Tang C, Tham LG, Lee PKK, Yang T, Li L. Coupled analysis of flow, stress and damage (FSD) in rock failure. *Int J Rock Mech Min Sci.* 2002;39(4):477–489.
41. Zhu W, Wei C. Numerical simulation on mining-induced water intrusions related to geologic structures using a damage-based hydromechanical model. *Environ Earth Sci.* 2010;62(1):43–54.
42. Xue Y, Gao F, Liu X. Effect of damage evolution of coal on permeability variation and analysis of gas outburst hazard with coal mining. *Nat Hazards.* 2015;79(2):999–1013.
43. Swami V, Settari A. A pore scale gas flow model for shale gas reservoir. *SPE Americas Unconventional Resources Conference.* Society of Petroleum Engineers; 2012.
44. Xue Y, Gao F, Gao Y, et al. Quantitative evaluation of stress-relief and permeability-increasing effects of overlying coal seams for coal mine methane drainage in Wulan coal mine. *J Nat Gas Sci Eng.* 2016;32:122–137.
45. Lu S, Zhang Y, Sa Z, Si S, Shu L, Wang L. Damage-induced permeability model of coal and its application to gas predrainage in combination of soft coal and hard coal. *Energy Sci Eng.* 2019;7(4):1–16.
46. Zhang H, Liu J, Elsworth D. How sorption-induced matrix deformation affects gas flow in coal seams: a new FE model. *Int J Rock Mech Min Sci.* 2008;45(8):1226–1236.
47. Zhang S, Liu J, Wei M, Elsworth D. Coal permeability maps under the influence of multiple coupled processes. *Int J Coal Geol.* 2018;187:71–82.
48. Chen T, Feng X-T, Cui G, Tan Y, et al. Experimental study of permeability change of organic-rich gas shales under high effective stress. *J Nat Gas Sci Eng.* 2019;64:1–14.
49. Cui G, Liu J, Wei M, Feng X, Elsworth D. Evolution of permeability during the process of shale gas extraction. *J Nat Gas Sci Eng.* 2018;49:94–109.
50. Liu J, Chen Z, Elsworth D, Qu H, Chen D. Interactions of multiple processes during CBM extraction: a critical review. *Int J Coal Geol.* 2011;87(3-4):175–189.
51. Liu J, Chen Z, Elsworth D, Miao X, Mao X. Evaluation of stress-controlled coal swelling processes. *Int J Coal Geol.* 2010;83(4):446–455.
52. Wang J, Elsworth D, Wu Y, Liu J, Zhu W, Liu Y. The influence of fracturing fluids on fracturing processes: a comparison between water, oil and SC-CO₂. *Rock Mech Rock Eng.* 2018;51(1):299–313.
53. Lu S, Zhang Y, Sa Z, Si S. Evaluation of the effect of adsorbed gas and free gas on mechanical properties of coal. *Environ Earth Sci.* 2019;78(6):218.
54. Zhou J, Wei J, Yang T, Zhu W, Li L, Zhang P. Damage analysis of rock mass coupling joints, water and microseismicity. *Tunn Undergr Space Technol.* 2018;71:366–381.
55. Zhu W, Wei C, Li S, Wei J, Zhang M. Numerical modeling on destress blasting in coal seam for enhancing gas drainage. *Int J Rock Mech Min Sci.* 2013;59(5):179–190.
56. Wang L, Chen Z, Wang C, Elsworth D, Liu W. Reassessment of coal permeability evolution using steady-state flow methods: the role of flow regime transition. *Int J Coal Geol.* 2019;211:103–110.
57. Li J, Zhang W, Luo X, Hu G. Paleokarst reservoirs and gas accumulation in the Jingbian field, Ordos Basin. *Mar Pet Geol.* 2008;25(4):401–415.
58. Xiao X, Zhao B, Thu Z, Song Z, Wilkins RWT. Upper paleozoic petroleum system, Ordos Basin, China. *Mar Pet Geol.* 2005;22(8):945–963.
59. Feng X, Zhang N, Chen X, Gong L, Lv C, Guo Y. Exploitation contradictions concerning multi-energy resources among coal, gas, oil, and uranium: a case study in the Ordos Basin (western north China craton and southern side of yinshan Mountains). *Energies.* 2016;9(2):119.
60. Multiphysics C. Application libraries. *Version 5.4.* Comsol; 2018.
61. Chen H, Cheng Y, Ren T, Zhou H, Liu Q. Permeability distribution characteristics of protected coal seams during unloading of the coal body. *Int J Rock Mech Min Sci.* 2014;71:105–116.
62. Zhang X, Wang J, Gao F, Ju Y. Impact of water, nitrogen and CO₂ fracturing fluids on fracturing initiation pressure and flow pattern in anisotropic shale reservoirs. *J Nat Gas Sci Eng.* 2017;45:291–306.
63. Bai M, Kendorski F, Van Roosendaal D. Chinese and North American high-extraction underground coal mining strata behaviour and water protection experience and guidelines. *Proceedings of the 14th International Conference on Ground Control in Mining.* 1995; 1995.